Available online at www.sciencedirect.com

ScienceDirect

www.elsevier.com/locate/jes

JES JOURNAL OF ENVIRONMENTAL SCIENCES

www.jesc.ac.cn

Effects of Al^{3+} doping on the structure and properties of goethite and its adsorption behavior towards phosphate

Wei Li[1], *Longjun Wang*[1], *Fan Liu*[1], *Xiaoliang Liang*[2], *Xionghan Feng*[1], *Wenfeng Tan*[1], *Lirong Zheng*[3], *Hui Yin*[1,2,*]

1. *Key Laboratory of Arable Land Conservation (Middle and Lower Reaches of Yangtse River) Ministry of Agriculture, College of Resources and Environment, Huazhong Agricultural University, Wuhan 430070, China*
2. *CAS Key Laboratory of Mineralogy and Metallogeny, Guangzhou Institute of Geochemistry, Chinese Academy of Sciences, Guangzhou 510640, China*
3. *Beijing Synchrotron Radiation Facility, Institute of High Energy Physics, Chinese Academy of Sciences, Beijing 100039, China*

ARTICLE INFO

Article history:
Received 3 August 2015
Revised 8 December 2015
Accepted 10 December 2015
Available online 1 February 2016

Keywords:
Goethite
Al substitution
XRD
XAFS
Adsorption

ABSTRACT

Al substitution in goethite is common in soils, and has strong influence on the structure and physicochemical properties of goethite. In this research, a series of Al-doped goethites were synthesized, and characterized by powder X-ray diffraction (XRD), transmission electron microscopy (TEM), X-ray photoelectron spectroscopy (XPS), Fourier transform infrared spectroscopy (FT-IR) and extended X-ray absorption fine structure (EXAFS) spectroscopy. The adsorption behavior of these samples towards PO_4^{3-} was also investigated. Characterization results demonstrated that increasing Al content in goethite led to a reduction in crystallinity, increase in specific surface area (SSA), and morphology change from needle-like to granular. Rietveld structure refinement revealed that the lattice parameter *a* remained almost constant and *b* slightly decreased, but *c* was significantly reduced, and the calculated crystal density increased. EXAFS analysis demonstrated that the Fe(Al)–O distance in the structure of the doped goethites was almost the same, but the Fe–Fe(Al) distance decreased with increasing Al content. Surface analysis showed that, with increasing Al content, the content of OH groups on the mineral surface increased. The adsorption of phosphate per unit mass of Al-doped goethite increased, while adsorption per unit area decreased owing to the decrease of the relative proportion of (110) facets in the total surface area of the minerals. The results of this research facilitate better understanding of the effect of Al substitution on the structure and properties of goethite and the cycling of phosphate in the environment.

Introduction

Iron (hydr)oxides are ubiquitous earth minerals that are found in 16 iron (hydr)oxide forms, with high adsorption capacities for toxic elements and degradation ability towards organic contaminants. Among them, goethite is the most ubiquitous and abundant iron oxide mineral (Liu et al., 1995, 1999; Yapp, 2001; Cornell and Schwertmann, 2003).

Cation substitution often occurs in the formation and transformation processes of goethite in soils, and Al

* *Corresponding author*. E-mail: yinhui666@mail.hzau.edu.cn (Hui Yin).

http://dx.doi.org/10.1016/j.jes.2015.12.013
1001-0742/

substitution is the most common phenomenon (Cornell and Schwertmann, 2003; Bazilevskaya et al., 2011). The substitution of Al in natural goethite can reach 33 mol% (Norrish and Taylor, 2006; Fitzpatrick and Schwertmann, 1982; Schwertmann and Carlson, 1994; Carlson, 1995; Cornell and Schwertmann, 2003). Due to the differences in properties between Al^{3+} and Fe^{3+}, such as ionic radius (Shannon, 1976) and electronegativity (Portier et al., 1994), Al substitution causes changes in the structure and physicochemical properties of goethite. Because the ionic radius of Al^{3+} (r = 0.535 Å) is smaller than that of Fe^{3+} (r = 0.645 Å) (Shannon, 1976), the incorporation of Al reduces the lattice parameters of goethite, as proven by previous studies (Thiel, 1963; Schwertmann et al., 1985; Krehula and Musić, 2010). Increasing Al incorporation into goethite leads to the formation of more structural defects (Gonzalez et al., 2002; Cornell and Schwertmann, 2003) and crystal surface active sites, such as OH groups (Wolska and Schwertmann, 1993). Meanwhile, the existence of Al restrains the crystal growth of goethite (Cornell and Schwertmann, 2003; Bazilevskaya et al., 2012), and promotes the transformation from polycrystallinity to monocrystallinity, the diminution of particles and the decrease of crystal length–width ratio (Schulze and Schwertmann, 1987; Maurice et al., 2000; Liu et al., 2012; Wang et al., 2014; Ma et al., 2015). In virtue of its higher ionic potential (Lide and Haynes, 2010), Al^{3+} is stronger than Fe^{3+} in terms of binding force to other ions, such as OH^-. This results in a higher dehydroxylation temperature in Al-doped goethite than in the pure material (Schulze and Schwertmann, 1984; Cambier, 1986; Ruan and Gilkes, 1995). Compared to pure goethite, Al-doped goethite has better chemical stability, as evidenced by the decrease in the dissolution rate in strong acids or strong reductants (Schwertmann, 1984; Cornell and Schindler, 1987; Torrent et al., 1987). The bioreductivity of Al-doped goethite is rather confusing, because the increase of Al substitution may lead to a decrease (Bousserrhine et al., 1999; Liu et al., 2001), increase (Maurice et al., 2000) or unchanged bioreductivity (Kukkadapu et al., 2001) for goethite under different conditions. Additionally, Al incorporation can also affect the magnetic properties of goethite (Fleisch et al., 1980; Murad and Schwertmann, 1983; Bazilevskaya et al., 2011).

Furthermore, Al substitution can also change the adsorption properties of goethite towards various nutrients, heavy metal(loid) cations and organic pollutants. The adsorption of phosphate is initially rapid, but then slows, ascribed to the diffusion into micropores or grooves (Barrow et al., 1981; Pena and Torrent, 1990; Nilsson et al., 1992; Strauss et al., 1997; Luengo et al., 2006). Previous studies showed that, in acidic or neutral mediums, each phosphate ion replaces two singly coordinated surface OH groups to form a bridging binuclear surface complex (Parfitt et al., 1975; Nanzyo, 1986; Torrent et al., 1990). For synthetic and natural goethites with a wide range of morphologies, the phosphate sorption capacity is essentially the same per unit area, due to the dominance of (110) facets in all the goethites (Cornell and Schwertmann, 2003). Compared with pure goethite, Al-doped goethite has larger specific surface area but lower adsorption rate for PO_4^{3-}, probably due to the steric hindrance effect of Al^{3+} cations (Ainsworth et al., 1985; Ainsworth et al., 1985). The introduction of Al in goethite enhances the adsorption of As(V), and inhibits the release of As from the mineral surface, owing to bioreductive dissolution (Silva et al., 2010). Al-doped goethite also shows good adsorption properties towards organic pollutants, such as the azo dye Eriochrome Black T (Wang et al., 2014). It also has high affinity and adsorption capacity for heavy metals in water or soils. For example, Ma et al. (2015) reported that the surface active site densities, adsorption capacity and affinity of Al-doped goethite are higher than those of pure goethite, and the desorption rate of Ni^{2+} on Al-doped goethite is much lower. Simply put, Al-doped goethite not only can change the bioavailability of phosphorus, but also has the capability to remediate heavy metals in contaminated water or soils.

Most previous studies about Al-doped goethite have mainly focused on the effects of Al doping on the structure of the resulting minerals (Schulze, 1984; Fazey et al., 1991; Schwertmann and Carlson, 1994; Pinney and Morgan, 2013a, 2013b; Wang et al., 2014). But the relationships between the changes of structural features and mineral properties remain poorly understood, *e.g.*, whether there is any modification in the crystal morphology and the content of surface hydroxyl groups with increasing Al substitution, and whether and how these modifications would affect the adsorption of phosphorus on the mineral surfaces. Therefore in this study, to elucidate the underlying relationships between the adsorption behaviors of PO_4^{3-} and the properties of Al-doped goethite, a series of Al-doped goethite samples were synthesized based on previous reports, and characterized by several modern techniques, *e.g.*, X-ray diffraction (XRD), Rietveld structure refinement, transmission electron microscopy (TEM), X-ray photoelectron spectroscopy (XPS), and extended X-ray absorption fine structure (EXAFS) spectroscopy. Investigation into the characteristics of Al-doped goethite from the aspects of crystal habits and surface groups can provide further insights into the mineralogy and geochemical behaviors of iron oxides, as well as the transfer and fates of soil nutrients and environmental pollutants.

1. Materials and methods

1.1. Al-doped goethite synthesis

Pre-determined amounts of $FeCl_2{\cdot}4H_2O$ and $AlCl_3{\cdot}6H_2O$ (Al/(Al + Fe) = 0–32%) were dissolved in 1 L deionized water bubbled with N_2 for 30 min to eliminate dissolved O_2. After that, 180 mL $NaHCO_3$ solution was added dropwise at a rate of 30–40 mL/min. The mixture was stirred in air for 48 hr until the slurry color was ochre. To remove the amorphous component, 30 mL ammonium oxalate solution (pH = 3.2) was added into the slurry. The mixture was shaken in the dark for 4 hr, and the amounts of Al and Fe in the amorphous component were measured. Then NH_4HCO_3 solution was used to remove the remaining ammonium oxalate, and the suspension was washed several times in deionized water. The obtained samples were dried at 40°C. Finally, the samples were ground carefully in an agate mortar, passed through a 100 mesh screen, and kept in polyethylene plastic tubes at room temperature. The obtained samples were labeled as Goe, AlG4, AlG8, AlG12, AlG16, AlG20, AlG24, AlG28 and AlG32, respectively.

1.2. Elemental analysis of Al-doped goethites

An accurately weighed 0.1000 g portion of each sample was added separately into 5 mL of 5 mol/L HCl, and heated on an electric hot plate until the particles were completely dissolved. The contents of Fe and Al in the solutions were measured by a NexION 350 inductively coupled plasma mass spectrometry (ICP-MS) spectrometers (PerkinElmer SCIEX).

1.3. Characterization

Powder X-ray diffraction analysis of Al-doped goethite samples was carried out on a Bruker D8 Advance diffractometer equipped with a LynxEye detector using Ni-filtered Cu K α radiation (λ = 0.15418 nm). The diffractometer was operated at a tube voltage of 40 kV and a current of 40 mA, with a step of 0.02° and a scan rate of 1°/min in the range of 15–90° 2θ. Based on the structure model (JCPDS 81-0464), Rietveld structure refinement was carried out by using the TOPAS software (Yin et al., 2012, 2015). The specific surface area (SSA) was measured with an Autosorb-1 standard physical adsorption analyzer (Quantachrome Autosorb-1). The samples were degassed at 110°C for 3 hr in vacuum to remove water and adsorbates. Then the nitrogen adsorption/desorption experiments were carried out at 77 K, with relative pressure (P/P_0) in the range of 10^{-6} to 0.9916 and 0.9916 to 0.0270, respectively. The multi-point BET method was used to calculate the SSA. The crystallite morphologies of samples were probed by a Philips-CM12 transmission electron microscope instrument at an acceleration voltage of 100 kV and emission current of 10 μA. After ultrasonic dispersion in anhydrous ethanol for several minutes, the sample was dropped on Cu mesh with C coating, and then dried at room temperature for TEM analysis. XPS experiments were carried out on a VG Multilab 2000 X-ray photoelectron spectrometer (Yin et al., 2012, 2013). The Fourier-transformed infrared spectroscopy (FT-IR) of Al-doped goethite samples was performed on a Bruker Vertex 70 FTIR spectrometer. 0.1 g of KBr was mixed with 0.001 g of each sample. Spectra were acquired using 256 scans with a resolution of 4 cm^{-1}. Spectral processing including baseline adjustment, smoothing and normalization was performed by using OPUS software.

1.4. XAFS analysis

The EXAFS spectroscopy of Al-doped goethite samples was performed on the 1W1B beamline at Beijing Synchrotron Radiation Facility at room temperature (Yin et al., 2012, 2013, 2014, 2015). Fe K-edge EXAFS data were collected in the energy range of 6953–7884 eV in transmission mode. A Fe metal foil reference spectrum was collected (absorption edge jump at 7112 eV) to calibrate the monochromator before every sample run.

Reduction and analysis of all EXAFS data were performed using IFEFFIT/SixPack (Ravel and Newville, 2005). For Fe K-edge spectra, averaged spectra were background-subtracted using the following parameters: E_0 = 7127 eV, R_{bkg} = 1.1 Å, and k-weight = 2. Structural parameters (R, CN, and Debye-Waller factor, σ^2) were obtained by fitting the experimental k^3-weighted EXAFS spectra to the standard EXAFS equation (Kelly et al., 2008). Phase and amplitude functions for single-scattering paths were calculated using FEFF7 (Rehr et al., 1992). The EXAFS fittings were conducted over a k range of 2–11 Å and an R range of 1–4 Å with an amplitude reduction factor ($S0^2$) of 0.80 (Yin et al., 2013). In all fits, the number of independent variables used was less than the number of independent data points. During Fourier transformation and EXAFS data fitting, a Hanning window was used.

1.5. Phosphate adsorption experiments

30 mg portions of the Al-doped goethite samples were added into a series of 50 mL polyethylene tubes, followed by the addition of 29.5 mL of KCl solution (0.1 mol/L). The suspension pH was adjusted to 4.00 ± 0.05 with 0.1 mol/L HCl or NaOH. Then, an aliquot of 0.5 mL of PO_4^{3-} solution with different concentrations (20–100 mmol/L) was added into the suspension. The mixtures were shaken at 250 r/min for 24 hr. After the reaction, the mixtures were centrifuged at 10,000 r/min for 10 min, and the supernatants were collected for PO_4^{3-} concentration analysis (Johnson and Pilson, 1972).

2. Results and discussion

2.1. Powder X-ray diffraction

2.1.1. Qualitative analysis

The powder XRD patterns of Al-doped goethite samples are presented in Fig. 1. All the diffraction peaks can be indexed to α-FeOOH (JCPDS 81-0464), suggesting that all the obtained samples had the goethite structure. With the increase of Al content, the intensity of diffraction peaks decreased, while the full width at half maximum (FWHM) increased. This implies that the crystallinity decreased after Al incorporation. Furthermore, some peaks shifted to higher angles, such as the 111 and 221 reflections. These results indicate that the replacement of Fe by Al changes the lattice parameters of goethite (Shannon, 1976; Schwertmann et al., 1977).

2.1.2. Rietveld structure refinement

The Rietveld structure refinement was conducted based on the goethite crystal model JCPDS: 81–0464 (Fig. 1, Tables 1 and 2). With the increase of Al content, the unit cell parameter a did not obviously change, while b slightly decreased. But c was gradually reduced from 3.029 Å for Goe to 2.994 Å for AlG32. The cell volume decreased from 139.28 $Å^3$ to 137.35 $Å^3$, whereas the calculated crystal density increased from 4.189 g/cm^3 to 4.248 g/cm^3. The data also indicate no significant change in Fe(Al)–O distance, but a gradual decrease in Fe–Me (Me = Fe, Al) distance, which is caused by the replacement of Fe with Al in the lattice (Shannon, 1976).

A linear relationship exists between the extent of Al substitution and the cell parameter c among these synthetic doped goethite samples (n = 9, R^2 = 0.9594, $p < 0.01$). Synthetic goethite samples obtained by different methods and natural goethites from various locations show different relationships between the Al substitution content and unit cell parameters. Both the Al-doped goethites synthesized by Thiel (1963) and

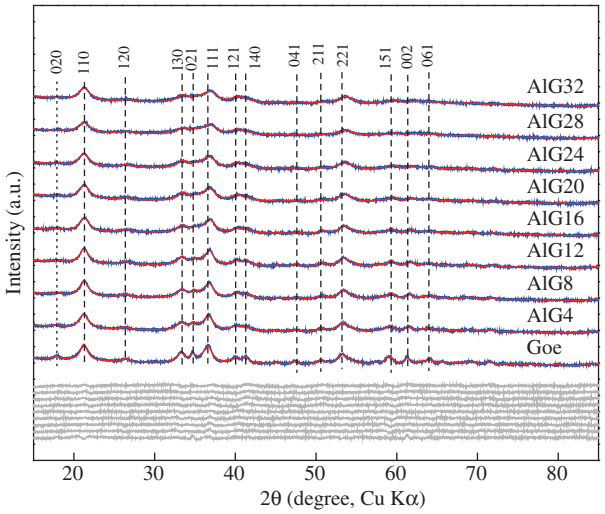

Fig. 1 – Rietveld structural refinement of Al-doped goethite samples. Blue lines are experimental data, red lines are calculated patterns and light gray lines are difference patterns.

Jonás and Solymár (1970) by different methods display a linear relationship between Al contents and the *a* and *b* edge lengths of the unit cell. However, Schwertmann and Carlson (1994) discovered that the goethite samples in tropical soils have a good linear relationship between the Al substitution extent and the *b*, *c* edge lengths, but not the goethite found in lake sediments. This is probably related to the environmental conditions for natural goethite formation.

2.2. Elemental analysis

The elemental analysis results for the Al-doped goethites are listed in Table 3. The Al content of in the precursor solutions was up to 27 mol%, but decreased after treatment with ammonium oxalate (pH = 3.2), which removed the amorphous component to generate crystalline goethite. The percentage of amorphous Fe in total Fe, labeled as Feo/Fet, in the pure goethite was 4.9%, which increased to 11.9%–15.0% in Al-doped goethites, indicating that Al incorporation inhibited the formation of goethite and(or) the transformation from the ferrihydrite precursor to goethite (Bazilevskaya et al., 2012). The Al contents in these Al-doped goethites calculated from d (111) and d (110) values (Schulze, 1984) agree well with the results of wet chemical analysis.

2.3. Morphology and specific surface area

The morphology of Al-doped goethites is shown in Fig. 2. The pure goethite showed the typical needle-like morphology (Ainsworth et al., 1985; Schwertmann and Kämpf, 1985). With increasing Al content, the goethite transformed from needle-like to rod-like, and then to granular. This indicates the inhibition of crystal growth by Al incorporation. The SSA of pure goethite was 98 m^2/g, increasing to 279 m^2/g for the sample with the highest Al content.

2.1. FT-IR

The FT-IR spectra of goethite samples were recorded in the mid infrared range between 4000 and 2000 cm^{-1}(Fig. 3). Two strong bands at 3484 and 3140 cm^{-1} were observed in this region. The band at 3484 cm^{-1} is attributed to the OH stretching vibration (Cornell and Schwertmann, 2003). The intensity of this peak increases with increasing Al content, indicating an increase in the content of hydroxyl groups on the doped goethite mineral surfaces.

2.2. XPS

2.2.1. O (1s)

The narrow scans for O (1s) are plotted in Fig. 4. The broadening of the spectra indicates the presence of several oxygen species. The peaks at 529.6 eV and 531.0 eV represent the oxygen in the lattice and in hydroxyl groups, respectively (Junta and Hochella, 1994; Rakovan et al., 1999; Wang et al., 2014). The binding energy (BE) of O (1s) decreases, which is attributed to the smaller electronegativity of Al^{3+} (χ = 1.5149) compared to Fe^{3+} (χ = 1.7053) (Shannon, 1976; Portier et al., 1994). The substitution of Fe by Al leads to the formation of Al–O–Fe bonds, and due to higher ionic bond character of Al–O bonds than Fe–O bonds, the electron cloud density of O cores in Al–O bonds increases, and the BEs shift to lower energy. With more Al^{3+} incorporated into the structure, the percentage of Al–O–Fe bonds increases, leading to a more obvious shift of BEs to the low energy region. In addition, there may be some water molecules adsorbed on the goethite surfaces. In order to quantify the relative percentages of various O species on the

Table 1 – Lattice parameters of Al-substituted goethites obtained by Rietveld structure refinement analysis

Sample	Unit cell Parameters (Å)			Cell volume ($Å^3$)	Crystal density (g/cm^3)	CrySize (nm)	R_{wp} (%)
	a	b	c				
Goe	4.618(5)	9.958 (9)	3.029 (3)	139.28 (23)	4.189 (7)	11.19 (8)	3.24
AlG4	4.612 (5)	9.954 (10)	3.022 (3)	138.74 (25)	4.206 (7)	9.24 (7)	2.34
AlG8	4.611 (5)	9.940 (10)	3.017 (3)	138.30 (25)	4.219 (8)	9.72 (8)	2.37
AlG12	4.610 (5)	9.936 (10)	3.010 (3)	137.92 (24)	4.231 (7)	10.51 (9)	2.39
AlG16	4.611 (7)	9.937 (12)	3.008(4)	137.81 (32)	4.234 (10)	9.31 (9)	2.24
AlG20	4.613 (8)	9.924 (15)	3.003 (4)	137.47 (36)	4.244 (11)	8.79 (9)	2.20
AlG24	4.612 (9)	9.932 (18)	3.002 (5)	137.48 (45)	4.244 (14)	8.76 (10)	2.25
AlG28	4.625 (17)	9.945 (31)	2.995 (9)	137.79 (79)	4.234 (24)	7.84 (15)	2.45
AlG32	4.618 (11)	9.936 (22)	2.994 (6)	137.35 (54)	4.248 (17)	8.14 (11)	2.30

Table 2 – The distances of Me-O and Me-Me bonds of Al-substituted goethites obtained by Rietveld structure refinement analysis (Me = Fe, Al).

Sample	MeO_6 octahedron (Me = Fe, Al)					Me(0)–Me(0)
	Me(0)–O1(3)	2× Me(0)–O1(2)	2× Me(0)–O2(2)	Me(0)–O2(0)	Average	
Goe	1.941 (8)	1.970 (5)	2.100 (5)	2.107 (8)	2.031	3.029
AlG4	1.889 (7)	1.984 (4)	2.133 (4)	2.074 (7)	2.033	3.023
AlG8	1.961 (8)	1.928 (5)	2.138 (5)	2.052 (7)	2.024	3.017
AlG12	1.975 (8)	1.915 (5)	2.136 (5)	2.043 (8)	2.020	3.011
AlG16	1.971 (8)	1.928 (6)	2.150 (5)	2.034 (8)	2.027	3.008
AlG20	1.958 (9)	1.929 (6)	2.142 (5)	2.040 (9)	2.023	3.003
AlG24	1.940 (10)	1.947 (7)	2.168 (6)	2.030 (10)	2.033	3.001
AlG28	1.844 (14)	2.022 (10)	2.255 (9)	1.976 (14)	2.062	2.997
AlG32	1.914 (11)	1.968 (8)	2.159 (7)	2.011 (11)	2.030	2.993

Table 3 – The chemical composition and SSA of Al-substituted goethite samples

Sample	Goe	AlG4	AlG8	AlG12	AlG16	AlG20	AlG24	AlG28	AlG28
Initial Al mol.%	0	4	8	12	16	20	24	28	32
Al mol.% before oxalate treatment	0	4.36	7.19	9.90	17.16	17.39	21.88	23.84	27.01
Al mol.% after oxalate treatment	0	6.07	9.97	14.41	15.11	21.38	24.82	29.38	38.75
Feo/Fet	4.9	13.2	12.2	13.0	14.5	11.9	14.2	15.0	14.5
Al mol.% deduced from d (111) and d (110) [a]	0	4.72	8.56	11.19	12.92	11.79	12.76	21.96	27.91
Al mol.% from XPS	0	–	6.89	–	–	18.32	–	–	30.22
SSA (m^2/g)	98	198	230	209	207	228	232	270	279

[a] The Al substitution extent is calculated by the following formula: $Al\% = 1730–572/(1/d(111)^2–1/d(110)^2)^{1/2}$ (Schulze, 1984).

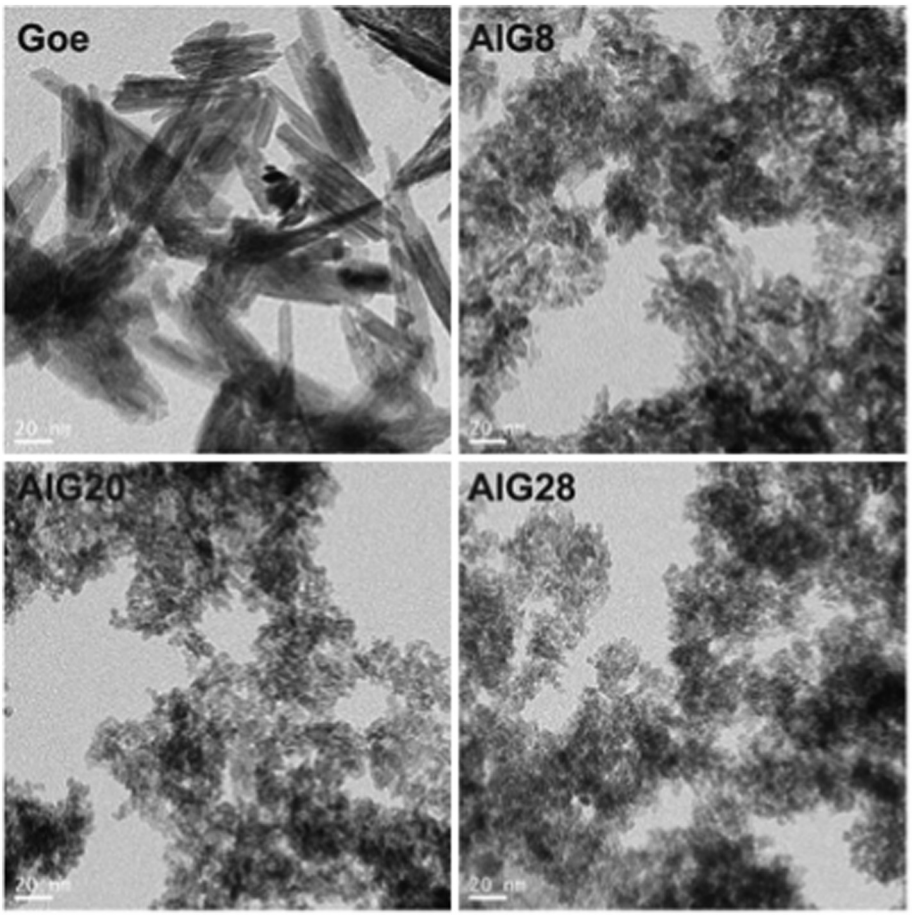

Fig. 2 – Transmission electron microscopy (TEM) images of Al-substituted goethites.

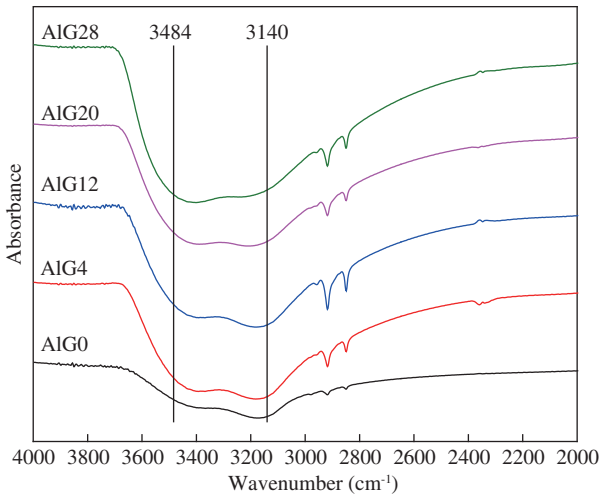

Fig. 3 – Fourier transform infrared spectroscopy (FT-IR) spectra of Al-doped goethite samples in the range of 4000–2000 cm^{-1}.

mineral surfaces, multipeak fitting of the O (1s) spectra was carried out (Yin et al., 2014, 2015). The fitting parameters and results are presented in Table 4 and Fig. 4, respectively, revealing approximately 42% O^{2-}, 48% OH^- and 10% H_2O on the surface of pure goethite. In Al-doped goethites, the contents of lattice O^{2-} and adsorbed water molecules decrease, while O in OH^- groups increases, with 59% OH^- on the mineral surfaces of AlG28. Our results are consistent with many previous studies reporting that the incorporation of Al^{3+} into the structure of goethites would produce structural defects, leading to an increase in the content of hydroxyl groups (Schulze and Schwertmann, 1984; Schwertmann and Carlson, 1994; Pinney and Morgan, 2013a,b; Wang et al., 2014).

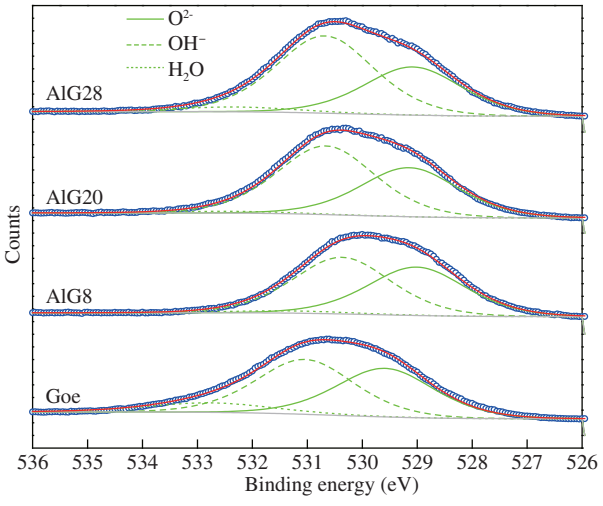

Fig. 4 – O (1s) X-ray photoelectron spectroscopy (XPS) spectra of Al-doped goethites. (The upper blue circles represent the observed data, the thick and red solid curve is the best fit, and the light gray solid line is Shirley background.)

Table 4 – Fitting parameters used for O (1s) spectra of Al-doped goethite samples.

Sample	Species	BE[a] (eV)	FWHM[b] (eV)	At.%
	O^{2-}	529.59	2.2	42.03
	OH^-	531.05	2.2	47.53
Goe	H_2O	532.76	2. 8	10.44
	O^{2-}	529.01	2.2	44.85
	OH^-	530.37	2.2	52.52
AlG8	H_2O	531.31	2. 8	2.63
	O^{2-}	529.29	2.2	40.84
	OH^-	530.89	2.2	57.26
AlG20	H_2O	532.56	2. 8	1.89
	O^{2-}	529.21	2.2	36.59
	OH^-	531.01	2.2	58.77
AlG28	H_2O	532.56	2. 8	4.64

[a] BE: binding energy.
[b] FWHM: full width at half maximum.

2.2.2. Fe (2p)

Fe (2p) XPS spectra of Al-doped goethites are plotted in Fig. 5. The BEs of Fe ($2p_{1/2}$) and Fe ($2p_{3/2}$) of pure goethite are 726.17 eV and 711.58 eV respectively, which are in line with the reported results (Mcintyre et al., 1977; Gupta and Sen, 1974; Rakovan et al., 1999; Biesinger et al., 2011). With increasing Al content, the BEs of Fe ($2p_{1/2}$) and Fe ($2p_{3/2}$) of doped samples also shift to the low-energy side. Compared with pure goethite, the BE of Fe ($2p_3/2$) for AlG28 shifts to lower energy by 1.5 eV. This can be ascribed to several possible reasons. Firstly, as described above, with increasing Al content, more electron cloud density shifts to the right side of the Al–O–Fe atomic chains, *i.e.*, to the Fe atom. Secondly, with the crystallinity of goethites greatly reduced after Al doping, more Fe atoms are exposed on the mineral surfaces. As Fe is more redox sensitive (Mcintyre et al., 1977; Lide and Haynes, 2010), a greater amount of Fe(III) on the surfaces of doped samples may be reduced to Fe^{2+} under X-ray

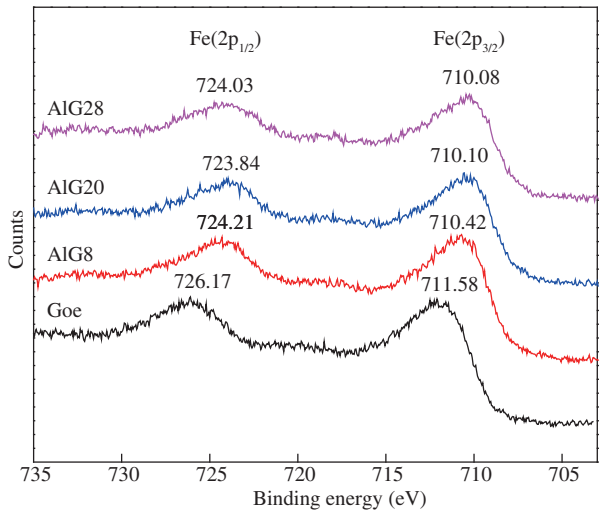

Fig. 5 – Fe (2p) X-ray photoelectron spectroscopy (XPS) spectra of Al-doped goethites.

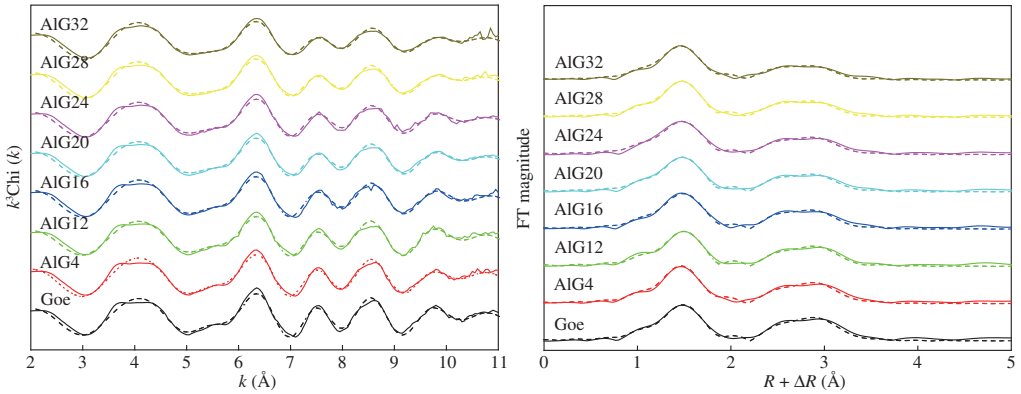

Fig. 6 – Fe K-edge EXAFS spectra (left) and Fourier transformed spectra (FTs, right) of Al-doped goethites (the solid lines are data and the dash lines are best fits). EXAFS: extended X-ray absorption fine structure.

illumination compared with the pure goethite mineral (Manceau et al., 2012; Yin et al., 2013).

2.3. Fe K-edge EXAFS spectroscopy

EXAFS spectroscopy probes the average local coordination environment around Fe atoms to a distance of 4 Å. The EXAFS spectra of Al-doped goethite samples are similar in amplitude, shape and frequency, indicating that they essentially have a very similar structure and Fe environment. This confirms that Al doping did not change the goethite structure.

The FT spectra of Al-doped goethite samples show three backscattering neighbors at $R + \Delta R$ of 1.5 Å, 2.6 Å and 3.2 Å. These three peaks correspond to first shell Fe–O distance and second shell edge-sharing Fe–Fe distance (Fe–Fe_E) and corner-sharing Fe–Fe distance (Fe–Fe_C). The best fits are indicated by the dotted lines in Fig. 6 and summarized in Table 5. With increasing Al content, the Fe–O, Fe–Fe_E, and Fe–Fe_C distances decrease slightly.

2.4. Phosphate adsorption experiment

The isothermal adsorption curves of PO_4^{3-} on the Al-doped goethite samples are shown in Fig. 7. They were found to follow L-type rules (Giles et al., 1960). From these curves, it can be seen qualitatively that the doped samples adsorb more PO_4^{3-} per unit mass than pure goethite. The results of Langmuir fittings of the adsorption data are demonstrated in Fig. 7 and Table 6. The adsorption capacity of PO_4^{3-} by pure goethite is 326.8 mmol/kg, which increases sharply to 711–712 mmol/kg for Al-doped goethite samples with increasing Al content, more than two times that of pure goethite. Furthermore, the constants (*K*) related to adsorption affinity also increase slightly for these doped samples versus Goe.

The increase of PO_4^{3-} adsorption capacities per unit weight for these Al-doped goethites can be ascribed to several reasons. On one hand, the Al incorporation causes structural defects in goethite (Schulze and Schwertmann, 1984; Gonzalez et al., 2002; Cornell and Schwertmann, 2003), leading

Table 5 – Structure parameters derived from the fitting of Fe K-edge EXAFS spectra of Al-doped goethite

	Goe	Al4	Al12	Al16	Al20	Al24	Al28	Al32
Fe–O								
CN	6	6	6	6	6	6	6	6
R (Å)	1.985(21)	1.982(19)	1.986 (18)	1.976 (18)	1.972 (18)	1.975 (15)	1.975 (16)	1.979 (15)
σ^2 (Å)	0.013 (1)	0.013 (1)	0.013 (1)	0.013 (1)	0.013 (1)	0.013 (1)	0.014 (1)	0.014 (1)
Fe–Fe_{E1}								
CN	2	2	2	2	2	2	2	2
R (Å)	2.993 (34)	2.992 (35)	2.984 (35)	2.984 (38)	2.978 (33)	2.976 (45)	2.980 (47)	2.978 (35)
σ^2 (Å)	0.0042 (39)	0.0048 (40)	0.0063 (50)	0.0075 (59)	0.0062 (40)	0.0092 (78)	0.010 (8)	0.0088 (60)
Fe–Fe_{E2}								
CN	2	2	2	2	2	2	2	2
R (Å)	3.181 (53)	3.182 (56)	3.167 (61)	3.163 (68)	3.167 (52)	3.137 (70)	3.153 (87)	3.154 (64)
σ^2 (Å)	0.0030 (65)	0.0038 (70)	0.0063 (93)	0.008 (11)	0.0051 (66)	0.010 (13)	0.012 (19)	0.010 (12)
Fe–Fe_C								
CN	4	4	4	4	4	4	4	4
R (Å)	3.384 (30)	3.383 (32)	3.38 (31)	3.374 (31)	3.373 (31)	3.369 (29)	3.3763 (3)	3.374 (28)
σ^2 (Å)	0.0060 (32)	0.0069 (35)	0.0089 (39)	0.0095 (42)	0.0084 (34)	0.011 (4)	0.013 (5)	0.011 (4)
E0(eV)	−6 (3)	−6 (3)	−6 (3)	−7 (3)	−7 (3)	−7 (2)	−7 (2)	−7 (2)
Chi sq	1013	1748	319	1648	198	1145	1204	193
R factor	0.013	0.014	0.012	0.011	0.011	0.009	0.010	0.008

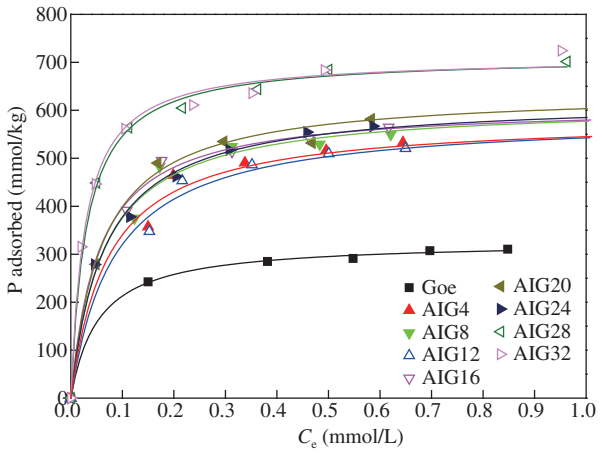

Fig. 7 – Isothermal adsorption curves of phosphate on Al-substituted goethite samples.

to an increase in surface active sites, such as OH groups (Wolska and Schwertmann, 1993). This is proved by the multipeak fitting of O (1s) XPS spectra (Table 4). On the other hand, the existence of Al inhibits the crystal growth of goethite, resulting in smaller crystal size and larger SSA (Schulze and Schwertmann, 1987; Maurice et al., 2000; Cornell and Schwertmann, 2003; Bazilevskaya et al., 2012; Liu et al., 2012; Wang et al., 2014; Ma et al., 2015). Nonetheless, after Al doping, the adsorption density of PO_4^{3-} decreases (Table 6), which is probably related to the morphology change.

According to the Scherrer formula (Patterson, 1939), the mean crystalline dimensions (MCDs) of (110) and (221) of Al-doped goethite samples are calculated and listed in Table 7. The results demonstrate that the MCDs of (110) and (221) decrease with increasing Al content. The original value of MCD (221)/MCD (110) of Goe is 0.97, but reduces to 0.76 with increasing Al content, indicating the decrease of the proportion of (110) facets in the specific surface areas. Many studies indicated that (110) is the main crystal facet in both synthetic and natural goethites, and the adsorption of PO_4^{3-} on goethite mainly occurs on the (110) facets (Torrent et al., 1990; Cornell and Schwertmann, 2003). Thus, the reduction of (110) facets is probably the main cause for the lower adsorption affinity of these Al-doped goethites towards PO_4^{3-}.

Table 6 – Langmuir fitting parameters for phosphate adsorption on Al-substituted goethites

Sample	Parameters			
	Q_{max}		K (L/mmol)	R^2
	(mmol/kg)	mmol/m^2		
Goe	326.8	3.33	18.7	0.9990
AlG4	584.1	2.95	14.0	0.9851
AlG8	613.7	2.67	15.8	0.9898
AlG12	587.9	2.81	12.0	0.9894
AlG16	610.9	2.95	18.5	0.9955
AlG20	639.9	2.81	16.5	0.9935
AlG24	623.0	2.69	15.4	0.9964
AlG28	712.4	2.64	32.8	0.9975
AlG32	710.5	2.55	36.5	0.9932

Table 7 – Mean crystalline dimensions (MCDs) of 110 and 221 crystal planes of Al-substituted goethites

Sample	MCD (110) (nm)	MCD (221) (nm)	MCD (221)/MCD (110)
Goe	7.93	7.73	0.97
AlG4	7.94	7.46	0.94
AlG8	8.86	7.63	0.86
AlG12	9.15	7.96	0.87
AlG16	7.70	6.54	0.85
AlG20	7.64	6.65	0.87
AlG24	7.66	5.94	0.78
AlG28	7.34	6.10	0.83
AlG32	7.29	5.57	0.76

3. Conclusions

In this study, Al-doped goethite samples were synthesized using a coprecipitation method. The incorporation of Al into the goethite structure leads to a decrease in crystallinity, and an increase in SSA. The replacement of Fe by Al causes a decrease in unit cell parameter *c* and cell volume, but an increase in calculated crystal density. The average Fe–O distances are almost unchanged, but the edge-sharing Fe–Fe(Al) distances gradually decrease. Of the O species on goethite surfaces, the contents of O in lattice and adsorbed water molecules decrease, while hydroxyl groups increase. The PO_4^{3-} adsorption capacity per weight on these Al-doped goethite samples increases gradually with increasing Al content. Additionally, the Al incorporation causes a reduction in the ratio of (110) facets in the total surface area, which leads to a decrease in the adsorption density of PO_4^{3-}. These results reveal the interaction mechanisms between iron oxides and Al^{3+} and also provide some new insights into the effects of iron oxides on the fates of nutrients and/or environment pollutants, suggesting that these Al-doped goethites can also be used as environment-friendly adsorption materials.

Acknowledgments

The authors gratefully thank the National Natural Science Foundation of China (Nos. 41401250, 41271253), open fund (No. KLMM20150107) of CAS Key Laboratory of Mineralogy and Metallogeny, Guangzhou Institute of Geochemistry, Chinese Academy of Sciences, and Huazhong Agricultural University doctoral start-up fund (No. 52902-0900206162) for financial support.

REFERENCES

Ainsworth, C.C., Sumner, M.E., Hurst, V.J., 1985. Effect of aluminum substitution in goethite on phosphorus adsorption:

I. Adsorption and isotopic exchange. Soil Sci. Soc. Am. J. 49 (5), 1142–1149.
Barrow, N.J., Madrid, L., Posner, A.M., 1981. A partial model for the rate of adsorption and desorption of phosphate by goethite. J. Soil Sci. 32 (3), 399–408.
Bazilevskaya, E., Archibald, D.D., Martinez, C.E., 2012. Rate constants and mechanisms for the crystallization of Al nano-goethite under environmentally relevant conditions. Geochim. Cosmochim. Acta 88 (7), 167–182.
Bazilevskaya, E., Archibald, D., Aryanpour, M., Kubicki, J., Martinez, C., 2011. Aluminum coprecipitates with Fe (hydr)oxides: does isomorphous substitution of Al^{3+} for Fe^{3+} in goethite occur? Geochim. Cosmochim. Acta 75, 4667–4683.
Biesinger, M.C., Payne, B.P., Grosvenor, A.P., Lau, L.W.M., Gerson, A.R., Smart, R.S., 2011. Resolving surface chemical states in XPS analysis of first row transition metals, oxides and hydroxides: Cr, Mn, Fe, Co and Ni. Appl. Surf. Sci. 257 (7), 2717–2730.
Bousserrhine, N., Gasser, U., Jeanroy, E., Berthelin, J., 1999. Bacterial and chemical reductive dissolution of Mn-, Co-, Cr-, and Al-substituted goethites. Geomicrobiol J. 16 (3), 245–258.
Cambier, P., 1986. Infrared study of goethites of varying crystallinity and particle size: II. Crystallographic and morphological changes in series of synthetic goethites. Clay Miner. 21 (2), 201–210.
Carlson, L., 1995. Aluminum substitution in goethite in lake ore. Bull. Geol. Soc. Finl. 67 (1), 19–28.
Cornell, R.M., Schindler, P.W., 1987. Photochemical dissolution of goethite in acid/oxalate solution. Clays Clay Miner. 35 (5), 347–352.
Cornell, R.M., Schwertmann, U., 2003. The Iron Oxides: Structure, Properties, Reactions, Occurrences and Uses. (2nd Ed). Wiley-VCH, Weinheim, Germany.
Fazey, P.G., O'Connor, B.H., Hammond, L.C., 1991. X-ray powder diffraction Rietveld characterization of synthetic aluminum-substituted goethite. Clay Clay Miner. 39 (3), 248–253.
Fitzpatrick, R.W., Schwertmann, U., 1982. Al-substituted goethite—an indicator of pedogenic and other weathering environments in South Africa. Geoderma 27 (4), 335–347.
Fleisch, J., Grimm, R., Grübler, J., Gütlich, P., 1980. Determination of the aluminum content of natural and synthetic alumogoethites using Mössbauer spectroscopy. J. Phys. Colloq. 41 (C1), 169,161–169,170.
Giles, C.H., MacEwan, T.H., Nakhwa, S.N., Smith, D., 1960. Studies in adsorption. Part XI. A system of classification of solution adsorption isotherms and its use in diagnosis of adsorption mechanisms and in measurement of specific surface area of solids. J. Chem. Soc. 3, 3973–3993.
Gilkes, H.D.R.J., 1995. Dehydroxylation of aluminous goethite: unit cell dimensions, crystal size and surface area. Clay Clay Miner. 43 (2), 196–211.
Gonzalez, E., Ballesteros, M.C., Rueda, E.H., 2002. Reductive dissolution kinetics of Al-substituted goethites. Clay Clay Miner. 50 (4), 470–477.
Gupta, R., Sen, S., 1974. Calculation of multiplet structure of core p-vacancy levels. Phys. Rev. B 10 (1), 71.
Johnson, D.L., Pilson, M.E.Q., 1972. Spectrophotometric determination of arsenite, arsenate, and phosphate in natural waters. Anal. Chim. Acta 58 (2), 289–299.
Jonás, K., Solymár, K., 1970. Preparation, X-ray, derivatographic and infrared study of aluminium-substituted goethites. Acta Phys. Acad. Sci. Hung. 66 (4), 383–394.
Junta, J.L., Hochella, M.F., 1994. Manganese (II) oxidation at mineral surfaces: a microscopic and spectroscopic study. Geochim. Cosmochim. Acta 58 (22), 4985–4999.
Kelly, S.D., Hesterberg, D., Ravel, B., 2008. Analysis of soils and minerals using X-ray absorption spectroscopy. Methods of soil analysis. Part5, pp. 387–463.
Krehula, S., Musić, S., 2010. Growth of uniform lath-like α-(Fe, Al)OOH and disc-like α-(Fe, Al)$_2O_3$ nanoparticles in a highly alkaline medium. Mater. Chem. Phys. 123 (1), 67–76.
Kukkadapu, R.K., Zachara, J.M., Smith, S.C., Fredrickson, J.K., Liu, C., 2001. Dissimilatory bacterial reduction of Al-substituted goethite in subsurface sediments. Geochim. Cosmochim. Acta 65 (17), 2913–2924.
Lide, D.R., Haynes, W.M., 2010. Handbook of Chemistry and Physics. (91st Ed). CRC Press/Taylor and Francis, Florida.
Liu, C., Kota, S., Zachara, J.M., Fredrickson, J.K., Brinkman, C.K., 2001. Kinetic analysis of the bacterial reduction of goethite. Environ. Sci. Technol. 35 (12), 2482–2490.
Liu, F., He, J., Colombo, C., Violante, A., 1999. Competitive adsorption of sulfate and oxalate on goethite in the absence or presence of phosphate. Soil Sci. 164 (3), 180–189.
Liu, F., He, J., Li, X.,.F.,.H.,.H., 1995. Chemical states of phosphorus adsorbed on goethite at various phosphate concentrations. Chin. Sci. Bull. 40 (6), 506–511.
Liu, H., Chen, T., Frost, R.L., Chang, D., Qing, C., Xie, Q., 2012. Effect of aging time and Al substitution on the morphology of aluminous goethite. J. Colloid Interface Sci. 385 (1), 81–86.
Luengo, C., Brigante, M., Antelo, J., Avena, M., 2006. Kinetics of phosphate adsorption on goethite: comparing batch adsorption and ATR-IR measurements. J. Colloid Interface Sci. 300 (2), 511–518.
Ma, M.G., Gao, H.Y., Sun, Y.B., Huang, M.S., 2015. The adsorption and desorption of Ni(II) on Al substituted goethite. J. Mol. Liq. 201, 30–35.
Manceau, A., Marcus, M.A., Grangeon, S., 2012. Determination of Mn valence states in mixed-valent manganates by XANES spectroscopy. Am. Mineral. 97, 816–827.
Maurice, P.A., Lee, Y.-J., Hersman, L.E., 2000. Dissolution of Al-substituted goethites by an aerobic *Pseudomonas mendocina var*. bacteria. Geochim. Cosmochim. Acta 64 (8), 1363–1374.
Mcintyre, N.S., Zetaruk, D.G., Chem., A., 1977. X-ray photoelectron spectroscopic studies of iron oxides. Anal. Chem. 49 (11), 1521–1529.
Murad, E., Schwertmann, U., 1983. The influence of aluminum substitution and crystallinity on the Mössbauer-spectra of goethite. Clay Miner. 18 (3), 301–312.
Nanzyo, M., 1986. Infrared spectra of phosphate sorbed on iron hydroxide gel and the sorption products. Soil Sci. Plant Nutr. 32 (1), 51–58.
Nilsson, N., Lövgren, L., Sjöberg, S., 1992. Phosphate complexation at the surface of goethite. Chem. Speciat. Bioavailab. 4 (4), 121–130.
Norrish, K., Taylor, R.M., 2006. The isomorphous replacement of iron by aluminum in soil goethites. J. Soil Sci. 12 (2), 294–306.
Parfitt, R.L., Atkinson, R.J., Smart, R.S.C., 1975. The mechanism of phosphate fixation by iron oxides. Soil Sci. Soc. Am. J. 39 (5), 837–841.
Patterson, A., 1939. The Scherrer formula for X-ray particle size determination. Phys. Rev. 56 (10), 978.
Pena, F., Torrent, J., 1990. Predicting phosphate sorption in soils of Mediterranean regions. Fertil. Res. 23 (3), 173–179.
Pinney, N., Morgan, D., 2013a. Ab initio study of structurally bound water at cation vacancy sites in Fe- and Al-oxyhydroxide materials. Geochim. Cosmochim. Acta 114 (4), 94–111.
Pinney, N., Morgan, D., 2013b. Thermodynamics of Al-substitution in Fe-oxyhydroxides. Geochim. Cosmochim. Acta 120, 514–530.
Portier, J., Campet, G., Etourneau, J., Tanguy, B., 1994. A simple model for the estimation of electronegativities of cations in different electronic states and coordinations. J. Alloys Compd. 209 (1), 285–289.
Rakovan, J., Becker, U., Hochella, M.F., 1999. Aspects of goethite surface microtopography, structure, chemistry, and reactivity. Am. Mineral. 84 (5–6), 884–894.

Ravel, B., Newville, M., 2005. ATHENA, ARTEMIS, HEPHAESTUS: data analysis for X-ray absorption spectroscopy using IFEFFIT. J. Synchrotron Radiat. 12, 537–541.
Rehr, J.J., Albers, R.C., Zabinsky, S.I., 1992. High-order multiple-scattering calculations of X-ray-absorption fine structure[J]. Phys. Rev. Lett 69 (23), 3397.
Schulze, D.G., 1984. The influence of aluminum on iron oxides.VIII. Unit-cell dimensions of Al-substituted goethites and estimation of Al from them. Clay Clay Miner. 32, 36–44.
Schulze, D., Schwertmann, U., 1984. The influence of aluminum on iron-oxides. X. Properties of Al-substituted goethites. Clay Miner. 19 (4), 521–539.
Schulze, D., Schwertmann, U., 1987. The influence of aluminium on iron oxides: XIII. Properties of goethites synthesised in 0.3 M KOH at 25 °C. Clay Miner. 22 (1), 83–92.
Schwertmann, U., 1984. The influence of aluminium on iron oxides: IX. Dissolution of Al-goethites in 6 M HCl. Clay Miner. 19 (1), 9–19.
Schwertmann, U., Carlson, L., 1994. Aluminum influence on iron oxides: XVII. Unit-cell parameters and aluminum substitution of natural goethites. Soil Sci. Soc. Am. J. 58 (1), 256–261.
Schwertmann, U., Fitzpatrick, R., 1977. Occurrence of lepidocrocite and its association with goethite in Natal soils. Soil Sci. Soc. Am. J. 41 (5), 1013–1018.
Schwertmann, U., Kämpf, N., 1985. Properties of goethite and hematite in kaolinitic soils of southern and central Brazil. Soil Sci. 139 (4), 344–350.
Schwertmann, U., Cambier, P., Murad, E., 1985. Properties of goethites of varying crystallinity. Clay Clay Miner. 33 (5), 369–378.
Shannon, R.t., 1976. Revised effective ionic radii and systematic studies of interatomic distances in halides and chalcogenides. Acta Crystallogr., Sect. A: Cryst. Phys., Diffr., Theor. Gen. Crystallogr. 32 (5), 751–767.
Silva, J., Mello, J.W., Gasparon, M., Abrahao, W.A., Ciminelli, V.S., Jong, T., 2010. The role of Al-goethites on arsenate mobility. Water Res. 44 (19), 5684–5692.
Strauss, R., Brümmer, G.W., Barrow, N.J., 1997. Effects of crystallinity of goethite: II. Rates of sorption and desorption of phosphate. Eur. J. Soil Sci. 48 (1), 101–114.
Thiel, R., 1963. Zum system α-FeOOH-α-AlOOH. Z. Anorg. Allg. Chem. 326 (1–2), 70–78.
Torrent, J., Barron, V., Schwertmann, U., 1990. Phosphate adsorption and desorption by goethites differing in crystal morphology. Soil Sci. Soc. Am. J. 54 (4), 1007–1012.
Torrent, J., Schwertmann, U., Barron, V., 1987. The reductive dissolution of synthetic goethite and hematite in dithionite. Clay Miner. 22 (3), 329–337.
Wang, H., Cao, S., Kang, F., Chen, R., Liu, H., Wei, Y., 2014. Effects of Al substitution on the microstructure and adsorption performance of α-FeOOH. J. Alloys Compd. 606, 117–123.
Wolska, E., Schwertmann, U., 1993. The mechanism of solid-solution formation between goethite and diaspore. Neues Jahrb. Mineral. Monatshefte 5, 213–223.
Yapp, C., 2001. Rusty relics of earth history: iron(III) oxides, isotopes, and surficial environments. Annu. Rev. Earth Planet. Sci. 29 (12), 165–199.
Yin, H., Feng, X., Tan, W., Koopal, L.K., Hu, T., Zhu, M., Liu, F., 2015. Structure and properties of vanadium(V)-doped hexagonal turbostratic birnessite and its enhanced scavenging of Pb^{2+} from solutions. J. Hazard. Mater. 288, 80–88.
Yin, H., Li, H., Wang, Y., Ginder-Vogel, M., Qiu, G.H., Feng, X.H., Liu, F., 2014. Effects of Co and Ni co-doping on the structure and reactivity of hexagonal birnessite. Chem. Geol. 381, 10–20.
Yin, H., Liu, F., Feng, X.H., Hu, T.D., Zheng, L.R., Qiu, G.H., Koopal, L.K., Tan, W.F., 2013. Effects of Fe doping on the structures and properties of hexagonal birnessites—comparison with Co and Ni doping. Geochim. Cosmochim. Acta 117, 1–15.
Yin, H., Tan, W.F., Zheng, L.R., Cui, H.J., Qiu, G.H., Liu, F., Feng, X.H., 2012. Characterization of Ni-rich hexagonal birnessite and its geochemical effects on aqueous Pb^{2+}/Zn^{2+} and As(III). Geochim. Cosmochim. Acta 93, 47–62.